

# The origin of unequal bond lengths in the $\tilde{C}^1B_2$ state of $SO_2$ : Signatures of high-lying potential energy surface crossings in the low-lying vibrational structure

G. Barratt Park,<sup>1,2, a)</sup> Jun Jiang,<sup>1</sup> and Robert W. Field<sup>1</sup>

<sup>1)</sup>Department of Chemistry, Massachusetts Institute of Technology, Cambridge, Massachusetts 02139

<sup>2)</sup>Current address: Institute for Physical Chemistry, University of Göttingen, Germany

The  $\tilde{C}^1B_2$  state of  $SO_2$  has a double-minimum potential in the antisymmetric stretch coordinate, such that the minimum energy geometry has nonequivalent SO bond lengths. The asymmetry in the potential energy surface is expressed as a staggering in the energy levels of the  $\nu'_3$  progression. We have recently made the first observation of low-lying levels with odd quanta of  $\nu'_3$ , which allows us—in the current work—to characterize the origins of the level staggering. Our work demonstrates the usefulness of low-lying vibrational level structure, where the character of the wavefunctions can be relatively easily understood, to extract information about dynamically important potential energy surface crossings that occur at much higher energy. The measured staggering pattern is consistent with a vibronic coupling model for the double-minimum, which involves direct coupling to the bound  $2^1A_1$  state and indirect coupling with the repulsive  $3^1A_1$  state. The degree of staggering in the  $\nu'_3$  levels increases with quanta of bending excitation, which is consistent with the approach along the  $\tilde{C}$  state potential energy surface to a conical intersection with the  $2^1A_1$  surface at a bond angle of  $\sim 145^\circ$ .

## I. INTRODUCTION

The  $\tilde{C}^1B_2$  state of  $SO_2$  has in recent years attracted considerable attention because of its role in  $SO_2$  photodissociation in the atmosphere.<sup>1–15</sup> However, earlier spectroscopy by Duchesne and Rosen<sup>16</sup>, Jones and Coon<sup>17</sup>, Brand and coworkers<sup>18,19</sup>, and by Hallin and Merer<sup>20</sup> focussed on the unusual low-lying vibrational structure below the dissociation limit, which was apparently the result of a distortion causing unequal SO bond lengths at the minimum-energy geometry. In the first paper of this series,<sup>21</sup> we report the first direct observations of  $\tilde{C}$ -state levels with  $b_2$  vibrational symmetry (odd quanta of  $\nu'_3$ ), and in the second paper,<sup>22</sup> we report a new force field. This new information provides us with the opportunity to make a more precise characterization of the origins of level staggering than was previously possible. In the current paper (the third in the series), we present a vibronic model to explain the distortions in the low-lying vibrational structure of the  $\tilde{C}$  state, and we show that the vibronic (pseudo Jahn-Teller) distortion near equilibrium cannot be disentangled from the predissociation dynamics that occur at much higher energy. That is, we use low-lying vibrational energy level structure—where the wavefunctions can be relatively easily understood—to provide qualitative information about dynamical interactions that occur at much higher energies, where the level structure is less easy to interpret.

Ever since the initial spectroscopic investigations, the  $\tilde{C}$  state of  $SO_2$  has attracted a steady stream of theoretical attention. Mulliken first suggested that an unsym-

metrical distortion of the S–O bond lengths might minimize antibonding in  $\tilde{C}$ -state  $SO_2$ ,<sup>23</sup> but Innes argued that the asymmetry in the potential is likely the result of vibronic interaction with a higher lying  $^1A_1$  state.<sup>24</sup> We believe Innes’s argument to be the best explanation, but his analysis relies on an incorrect assignment of the  $\nu'_3$  fundamental level by Ivanco and the derived parameters imply an unreasonably low energy for the perturbing electronic state. References 4, 25, and 26 report *ab initio* calculations for the  $\tilde{C}$  state that reproduce the observed double-minimum potential energy surface. The low-lying vibrational structure of the  $\tilde{C}$  state has been calculated using an empirical potential obtained using an exact quantum mechanical Hamiltonian,<sup>11</sup> and from a scaled *ab initio* potential energy surface.<sup>26</sup> Both of these calculations are in excellent qualitative agreement with our observed staggering pattern, indicating that the asymmetry in the PES is well reproduced by the calculations.

Due to the importance of  $SO_2$  photodissociation in atmospheric chemistry, extensive experimental and theoretical work has focussed on the dissociative region of the  $\tilde{C}$ -state PES above the dissociation limit, where the  $\tilde{C}$  ( $1^1B_2$ ) state undergoes a weakly avoided crossing with the  $2^1A_1$  state and has a seam of intersection with the  $1^3A_1$  state ( $3^1A'$  and  $2^3A'$  in  $C_s$ ).<sup>1–10,12,13,15,25–32</sup> However, we are not aware of any detailed theoretical investigation of the  $q_3$ -mediated vibronic coupling between the  $\tilde{C}$  ( $1^1B_2$ ) level and the higher-lying  $2^1A_1$  level in the diabatic basis.

In the current work, we analyze the low-lying level structure of the  $\tilde{C}$  state in terms of a vibronic interaction model—inspired by the classic model of Innes<sup>24</sup>—which indicates that the interaction of the  $\tilde{C}$  state with the quasi-bound  $2^1A_1$  state is probably influenced indirectly by the higher lying repulsive state,  $3^1A_1$ . Our

<sup>a)</sup>Electronic mail: barratt.park@mpibpc.mpg.de

model is consistent with currently available theoretical results.<sup>4,8,25,26,30–34</sup> The success of our model demonstrates the use of low-lying features on the potential energy surface to obtain qualitative information about dynamics that emerge at much higher energies. This is an advantageous strategy in polyatomic molecules, because within a given electronic state, the complexity of the vibrational wavefunctions increases rapidly with energy. Low-lying vibrational fundamentals and overtones of small polyatomic molecules are usually well resolved and are often—to a good approximation—well described by normal mode quantum numbers in the product basis of harmonic oscillators. At high quanta of vibrational excitation, however, the vibrational eigenstates can usually only be described using a complicated linear combination of basis states, due to the increasing density of interacting basis states, leading ultimately to dynamics dominated by rapid intramolecular vibrational redistribution. In the  $\tilde{C}$  state of  $\text{SO}_2$ , the singlet avoided crossing occurs at  $\sim 8000 \text{ cm}^{-1}$  above the  $\tilde{C}$ -state origin, where a detailed interpretation of the vibrational level structure is not yet possible. However, the avoided crossing is related to the asymmetry near equilibrium, because both phenomena arise due to interactions among the same set of electronic states. Therefore, we can use the low-lying vibrational structure to extract qualitative information about higher-lying surface crossings.

## II. VIBRATIONAL LEVEL STRUCTURE

The observed vibrational origins in the  $\text{SO}_2$   $\tilde{C}$  state up to  $1600 \text{ cm}^{-1}$  above the  $\tilde{C}(0,0,0)$  zero-point level are given in Tables VII and VIII of Ref. 21. In Fig. 1, the energy level patterns are plotted for progressions in  $\nu_3$ . Due to the low barrier at the  $\text{C}_{2v}$  geometry, levels with a single quantum of  $\nu_3$  are significantly depressed in frequency, but the magnitude of the odd/even level staggering decreases rapidly with increasing  $\nu_3$ , as the vibrational energy becomes large relative to the  $\sim 100 \text{ cm}^{-1}$  barrier. We can define a parameter to characterize the degree of  $\nu_3$  staggering as a function of the other vibrational quanta,  $\nu_1$  and  $\nu_2$ :

$$\Delta\omega_s(\nu_1, \nu_2) = \frac{T(\nu_1, \nu_2, 0) + T(\nu_1, \nu_2, 2)}{2} - T(\nu_1, \nu_2, 1), \quad (1)$$

where  $T$  denotes the vibrational term energy and the notation  $(\nu_1, \nu_2, \nu_3)$  is used for the vibrational quantum numbers. Equation 1 gives the energy by which the *expected* harmonic energy of  $(\nu_1, \nu_2, 1)$ —which would be halfway between  $(\nu_1, \nu_2, 0)$  and  $(\nu_1, \nu_2, 2)$ —is higher than the *observed* energy of  $(\nu_1, \nu_2, 1)$ , see inset of Figure 2. A larger value of  $\Delta\omega_s$  indicates an increased amount of staggering and a higher effective barrier height. The value of  $\Delta\omega_s$  is plotted as a function of  $\nu_1$  and  $\nu_2$  in Figure 2. The value of  $\Delta\omega_s$  increases linearly with  $\nu_2$  but decreases when one quantum of  $\nu_1$  is added. As we will discuss Sec.

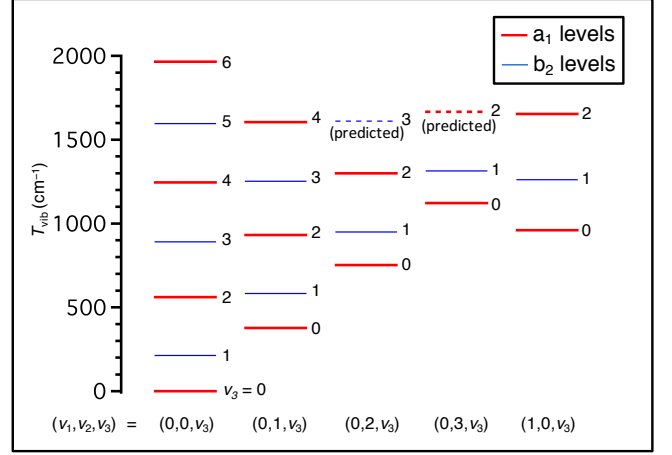


FIG. 1. The low-lying vibrational level structure of the  $\tilde{C}$  state of  $\text{SO}_2$  is shown, arranged as progressions in  $\nu_3$ .

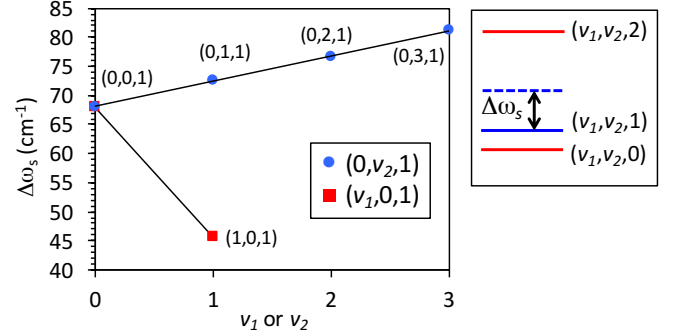


FIG. 2. The staggering parameter,  $\Delta\omega_s$ , defined in Eq. (1), is plotted as a function of  $\nu_1$  and  $\nu_2$ . The parameter, shown schematically in the right panel of the figure, is related to the effective barrier height at the  $\text{C}_{2v}$  geometry. It increases linearly with  $\nu_2$  as the  $\tilde{C}$ -state PES approaches a conical intersection with the  $2^1\text{A}_1$  potential at a bending angle of  $\sim 145^\circ$ , which is consistent with a vibronic model for the double-well potential.

III, the increase in  $\Delta\omega_s$  with  $\nu_2$  is consistent with a vibronic coupling model for the double-well potential, in which the asymmetry results from  $q_3$ -mediated interaction between the diabatic  $1^1\text{B}_2$  ( $\tilde{C}$ ) state and the  $2^1\text{A}_1$  state.

## III. INTERACTION OF THE $\tilde{C}$ STATE WITH $2^1\text{A}_1$

The avoided crossing between the  $1^1\text{B}_2$  ( $\tilde{C}$ ) and  $2^1\text{A}_1$  states has been extensively investigated at  $\text{C}_s$  geometries along the  $\text{SO}_2(\tilde{C}) \rightarrow \text{SO} + \text{O}$  photodissociation pathway.<sup>4,8,9,12,13,26,33</sup> The  $\tilde{C}$  state correlates diabatically to the excited singlet  $\text{SO}(^1\Delta) + \text{O}(^1\text{D})$  photodissociation products. However, the higher-lying  $2^3\text{A}'$  and  $3^1\text{A}'$  ( $1^3\text{A}_1$  and  $2^1\text{A}_1$  in  $\text{C}_{2v}$ ) states both appear to correlate to the ground state triplet  $\text{SO}(^3\Sigma^-) + \text{O}(^3\text{P})$  product



or  $b$ , respectively:

$$\begin{aligned}
\mathbf{H} &= \mathbf{H}_0 + \mathbf{H}' \\
\mathbf{H}_0 &= \omega_3 \left( \hat{N} + \frac{1}{2} \right) |\psi_a^{\text{el}}\rangle \langle \psi_a^{\text{el}}| \\
&\quad + \left[ \frac{1}{2} \omega'_3 \left( \frac{\omega'_3}{\omega_3} + \frac{\omega_3}{\omega'_3} \right) \left( \hat{N} + \frac{1}{2} \right) + D_{ab} \right] |\psi_b^{\text{el}}\rangle \langle \psi_b^{\text{el}}| \\
\mathbf{H}' &= \lambda_{ab} \mathbf{q}_3 (|\psi_a^{\text{el}}\rangle \langle \psi_b^{\text{el}}| + |\psi_b^{\text{el}}\rangle \langle \psi_a^{\text{el}}|) \\
&\quad + \frac{1}{4} \omega'_3 \left( \frac{\omega'_3}{\omega_3} - \frac{\omega_3}{\omega'_3} \right) (\hat{a}_3 \hat{a}_3 + \hat{a}_3^\dagger \hat{a}_3^\dagger) |\psi_b^{\text{el}}\rangle \langle \psi_b^{\text{el}}|,
\end{aligned} \tag{2}$$

where  $D_{ab}$  gives the energy spacing between the electronic states,  $\lambda_{ab}$  is a vibronic coupling constant, and  $\omega'_3$  is the harmonic frequency of the upper electronic state.  $\hat{N}$  and  $\hat{a}$  represent the quantum harmonic oscillator number operator and annihilation operator, respectively. Diagonal matrix elements are given by  $\mathbf{H}_0$ . The first term in  $\mathbf{H}'$  gives rise to  $\Delta v_3 = \pm 1$  matrix elements that couple levels of different electronic states, and the second term gives rise to  $\Delta v_3 = \pm 2$  matrix elements in the excited electronic state, which arise from the rescaling of the dimensionless  $\mathbf{p}$  and  $\mathbf{q}$  operators for the vibrational frequency of the upper state. In other words, this term must be included because the excited state, with harmonic frequency  $\omega'_3$ , is being described in the basis of a harmonic oscillator of a different frequency,  $\omega_3$ . Note that this last term vanishes for the simplifying case when  $\omega'_3 = \omega_3$ , and the  $\frac{1}{2}(\omega'_3/\omega_3 + \omega_3/\omega'_3)$  scaling factor in  $\mathbf{H}_0$  becomes unity. The Hamiltonian in Eq. 2 gives rise to matrix elements of the form

$$\langle \psi_a^{\text{el}} \psi_n^{\text{vib}} | \mathbf{H} | \psi_a^{\text{el}} \psi_n^{\text{vib}} \rangle = \omega_3 \left( n + \frac{1}{2} \right) \tag{3a}$$

$$\begin{aligned}
&\langle \psi_b^{\text{el}} \psi_n^{\text{vib}} | \mathbf{H} | \psi_b^{\text{el}} \psi_n^{\text{vib}} \rangle \\
&= \frac{1}{2} \omega'_3 \left( \frac{\omega'_3}{\omega_3} + \frac{\omega_3}{\omega'_3} \right) \left( n + \frac{1}{2} \right) + D_{ab}
\end{aligned} \tag{3b}$$

$$\begin{aligned}
&\langle \psi_b^{\text{el}} \psi_{n\pm 2}^{\text{vib}} | \mathbf{H} | \psi_b^{\text{el}} \psi_n^{\text{vib}} \rangle \\
&= \frac{1}{4} \omega'_3 \left( \frac{\omega'_3}{\omega_3} - \frac{\omega_3}{\omega'_3} \right) \sqrt{(n \pm 1)(n + 1 \pm 1)}
\end{aligned} \tag{3c}$$

$$\langle \psi_a^{\text{el}} \psi_{n\pm 1}^{\text{vib}} | \mathbf{H} | \psi_b^{\text{el}} \psi_n^{\text{vib}} \rangle = \lambda_{ab} \sqrt{\frac{1}{2} \left( n + \frac{1}{2} \pm \frac{1}{2} \right)}, \tag{3d}$$

as well as the complex conjugate of Eq. 3d.

We fit the frequencies of the  $(0, 0, v_3)$  progression to the Hamiltonian in Eq. 2 by truncating and diagonalizing the matrix. In order to ensure a physically realistic result, we constrain  $D_{ab}$  to the calculated difference in energy for vertical excitation of  $\text{SO}_2$  to the  $\tilde{\text{C}}$   $1^1\text{B}_2$  and the  $2^1\text{A}_1$  states from Ref. 8, and we constrained  $\omega_3$  to a “normal” value (we use the  $\omega_3$  frequency in the ground electronic state.) The results are shown in Table I. The  $(0, 0, v_3)$  progression is qualitatively reproduced by the model, although the fit is far from spectroscopically accurate. It is possible to achieve much better agreement (rms error  $1.87 \text{ cm}^{-1}$ ) by removing the constraints on

TABLE I. Results of a fit of the measured  $(0, 0, v_3)$  vibrational term energies to the one-dimensional vibronic coupling model of Eq. 2. The values of  $D_{ab}$  and  $\omega_3$  were constrained. The model is qualitative in nature, and we estimate the uncertainty in the parameters to be on the order of 30%. All values are given in  $\text{cm}^{-1}$  units.

Level	$T_{\text{vib}}(\text{exp})$	$T_{\text{vib}}(\text{fit})$
(0,0,1)	212.575	227.76
(0,0,2)	561.232	544.82
(0,0,3)	890.939	886.76
(0,0,4)	1245.469	1249.75
(0,0,5)	1595.794	1626.53
Parameters: $D_{ab} = 14760$ $\omega_3 = 1362$		
$\lambda_{ab} = 2297$ $\omega'_3 = 451.7$		

$D_{ab}$  and  $\omega_3$ , but the best fit values are much lower and higher, respectively, than our physically reasonable estimate. The simplistic one-dimensional vibronic coupling model ignores all other sources of anharmonicity, and is therefore not expected to give quantitative results. The best fit parameters underestimate the degree of level staggering, so it is possible that the vibronic interaction parameter  $\lambda_{ab} = 2297 \text{ cm}^{-1}$  is too low. However the ability of the model to qualitatively reproduce the  $(0, 0, v_3)$  level structure is good evidence for the presence of vibronic coupling, as first suggested by Innes.<sup>24</sup>

At first glance, the extremely low harmonic frequency,  $\omega'_3$ , obtained for the perturbing state might appear alarming. However, this low value of  $\omega'_3$  is crucial to the success of the model, and the explanation is straightforward. As mentioned in Section III, calculations suggest that the  $2^1\text{A}_1$  state is only quasi-bound. An avoided crossing with  $3^1\text{A}_1$ , which lies only  $\sim 0.5 \text{ eV}$  higher in energy, causes  $2^1\text{A}_1$  to become dissociative, correlating to the ground state  $\text{SO}(\Sigma^-) + \text{O}(\text{P})$  dissociation channel. Such an interaction could dramatically decrease the effective  $\omega'_3$  harmonic frequency of  $2^1\text{A}_1$ , because of mode softening along the dissociative coordinate. Thus, the same set of interactions that contribute to photodissociation of  $\text{SO}_2$  via singlet vibronic coupling at around  $48,000 \text{ cm}^{-1}$  also appear to be the direct cause of the unusual vibrational structure near the bottom of the  $\tilde{\text{C}}$ -state potential energy surface at around  $43,000 \text{ cm}^{-1}$ . This underscores the importance of understanding the low-lying vibrational level structure, where the spectroscopic information is comparatively simple, yet mechanistic information can be gleaned about dynamics that appear at much higher energy.

To illustrate more explicitly the three-state system that gives rise to the structure near the bottom of the  $\tilde{\text{C}}$ -state potential energy surface, we construct a toy one-dimensional model for the adiabatic potential energy curves of the bound  $\tilde{\text{C}}$   $1^1\text{B}_2$  and  $2^1\text{A}_1$  states and the higher-lying repulsive  $3^1\text{A}_1$  ( $4^1\text{A}'$ ) state. In the diabatic

basis, the toy Hamiltonian is

$$\mathbf{H} = \begin{pmatrix} M_a & V_{ab} & 0 \\ V_{ab} & M_b & V_{bc} \\ 0 & V_{bc} & M_c \end{pmatrix}, \quad (4)$$

where the matrix elements have the form

$$\begin{aligned} V_{ab} &= \lambda_{ab} q_3, & V_{bc} &= \lambda_{bc}, \\ M_a &= \frac{1}{2} \omega_3 q_3^2, & M_b &= \frac{1}{2} \omega_3 q_3^2 + D_{ab}, \\ M_c &= (D_{ac} - D_0) \exp(-|q_3/l|) + D_0. \end{aligned}$$

We assume that the  $V_{ab}$  interaction is vibronic in nature since it couples states of different electronic symmetry in  $C_{2v}$  ( $^1A_1$  to  $^1B_2$ ), but the  $V_{bc}$  interaction is assumed to be vibrationally independent since it couples states of the same ( $^1A_1$ ) electronic symmetry. The parameter  $D_0$  is the energy of the ground state dissociation channel, and  $D_{ab}$  and  $D_{ac}$  characterize the energy spacing between the  $\tilde{C}$  state and the two higher lying electronic states. The  $l$  parameter is the characteristic decay length of the repulsive state. The one-dimensional diabats and adiabats of the toy model, obtained with ‘best guess’ values of the parameters, are plotted in Figure 4a. In Sec. III B, we will use this qualitative figure as a starting point to extend the discussion of the vibronic interaction to other vibrational coordinates.

### B. Evidence for increased effective barrier height along the approach to conical intersection

The  $\tilde{C}$   $^1B_2$  and  $\tilde{D}$   $^2A_1$  states belong to different symmetry species in  $C_{2v}$ , but they both correlate to  $^1A'$  in  $C_s$  geometries. Therefore, although the crossing is avoided at  $C_s$  geometries, the levels may cross in  $C_{2v}$  geometries, resulting in a seam of conical intersection. Theoretical investigations<sup>8,26</sup> have reported the lowest seam of intersection to occur at bond angles between  $145$ – $150^\circ$  in  $C_{2v}$  for bond lengths near the equilibrium value. This is a much wider bond angle than the  $\sim 104^\circ$  equilibrium bond angle of the  $\tilde{C}$  state. If the double-minimum potential of the  $\tilde{C}$  state is caused by  $q_3$ -mediated vibronic interactions with  $2^1A_1$  around the  $C_{2v}$  equilibrium, we expect the effect to become very strong at geometries near the conical intersection, since the energy denominator for the interaction vanishes at the conical intersection. As quanta of  $v_2$  are added, the vibrational wavefunction has increased amplitude at wider bond angles, as indicated by the large negative value of the  $\alpha_2^A$  rotation-vibration constant (i.e. the effective  $A$  constant increases as the bond angle is widened towards linearity—see Table IX and Figure 6b of Ref. 21.) Therefore, it is highly likely that the increase in  $\Delta\omega_s$  as a function of  $v_2$  (Figure 2) is a direct consequence of the approach to the seam of conical intersection. To illustrate this point, we calculate the toy model adiabatic potential energy curves from Eq. (4) with reduced values of the energy difference,  $D_{ab}$ . Figure 4(b) shows the

result when  $D_{ab}$  is equal to half of its equilibrium value ( $104^\circ < \angle OSO < 145^\circ$ ), and Fig. 4(c) shows the result at the conical intersection ( $\angle OSO = 145^\circ$ ), where  $D_{ab} = 0$ .

Without more detailed knowledge of the  $2^1A_1$  potential energy surface, it is difficult to make a quantitative prediction of the expected trend in  $\Delta\omega_s$  as a function of  $v_2$ , which results from the approach to conical intersection. However, we can estimate the trend by building a simple model. Our approach will be to approximate the vibrationally-averaged energy difference between the  $\tilde{C}$   $^1B_2$  and the  $2^1A_1$  surfaces as a function of  $v_2$  bending quanta in the  $\tilde{C}$  state. We will then use the vibrationally averaged energy difference to calculate  $\Delta\omega_s(v_2)$  from the one-dimensional vibronic model (Eq. (2)).

According to the calculations in Refs. 4 and 8, the  $2^1A_1$  state appears to have a wide equilibrium bond angle ( $\sim 160^\circ$ ), but a  $\omega_2$  bending frequency similar to that of the  $\tilde{C}$  state. We therefore model the one-dimensional bending potential energy curves of the upper ( $V_b$ ) and lower ( $V_a$ ) states as

$$\begin{aligned} V_a(q_2) &= \frac{1}{2} \omega_2 q_2^2 + \frac{1}{6} \phi_{222} q_2^3 + \frac{1}{24} \phi_{2222} q_2^4 \\ V_b(q_2) &= \frac{1}{2} \omega_2 (q_2 - \delta)^2 + D \end{aligned} \quad (5)$$

$$\begin{aligned} \omega_2 &= 392.28 & \phi_{222} &= -85.375 \\ \phi_{2222} &= 8.276 & \delta &= 3.0 & D &= 13059, \end{aligned}$$

where values for  $\omega_2$ ,  $\phi_{222}$ , and  $\phi_{2222}$ , in  $\text{cm}^{-1}$ , are taken from our  $\tilde{C}$ -state force field fit reported in Part II of this series,<sup>22</sup> and  $\delta$  gives the approximate equilibrium displacement of the excited  $2^1A_1$  state,  $160^\circ - 104^\circ = 56^\circ$ , in dimensionless normal mode coordinates obtained from the same force field. The value of  $D$  (in  $\text{cm}^{-1}$ ) was chosen in order to make the energy difference between the displaced potential energy curves match the value  $D_{ab} = 14760 \text{ cm}^{-1}$  given in Table I near the geometry of the  $\tilde{C}$ -state equilibrium. We calculate the low-lying one-dimensional vibrational wavefunctions,  $\psi_{v_2}(q_2)$ , of  $V_a$  using discrete variable representation, and we integrate to obtain the vibrationally averaged expectation value for the energy difference,

$$\langle D_{ab}(v_2) \rangle = \int_{-\infty}^{\infty} \psi_{v_2}(q_2) [V_b(q_2) - V_a(q_2)] \psi_{v_2}(q_2) dq_2. \quad (6)$$

The resulting values of  $\langle D_{ab}(v_2) \rangle$  are then substituted into the vibronic coupling model (Eq. (2)), in order to calculate the staggering parameter  $\Delta\omega_s$ , defined in Eq. (1). The results are tabulated in Table II. The model (Eq. (5–6)) predicts that the energy difference parameter  $\langle D(v_2) \rangle$  decreases linearly by  $\sim 130 \text{ cm}^{-1}$  per quantum of bend excitation. Although the parameters of our harmonic, one-dimensional vibronic model (Table I), underestimate the staggering parameter,  $\Delta\omega_s$ , by approximately  $23 \text{ cm}^{-1}$ , the overall interaction model reproduces the observed trend in  $\Delta\omega_s(0, v_2)$  very well. The model

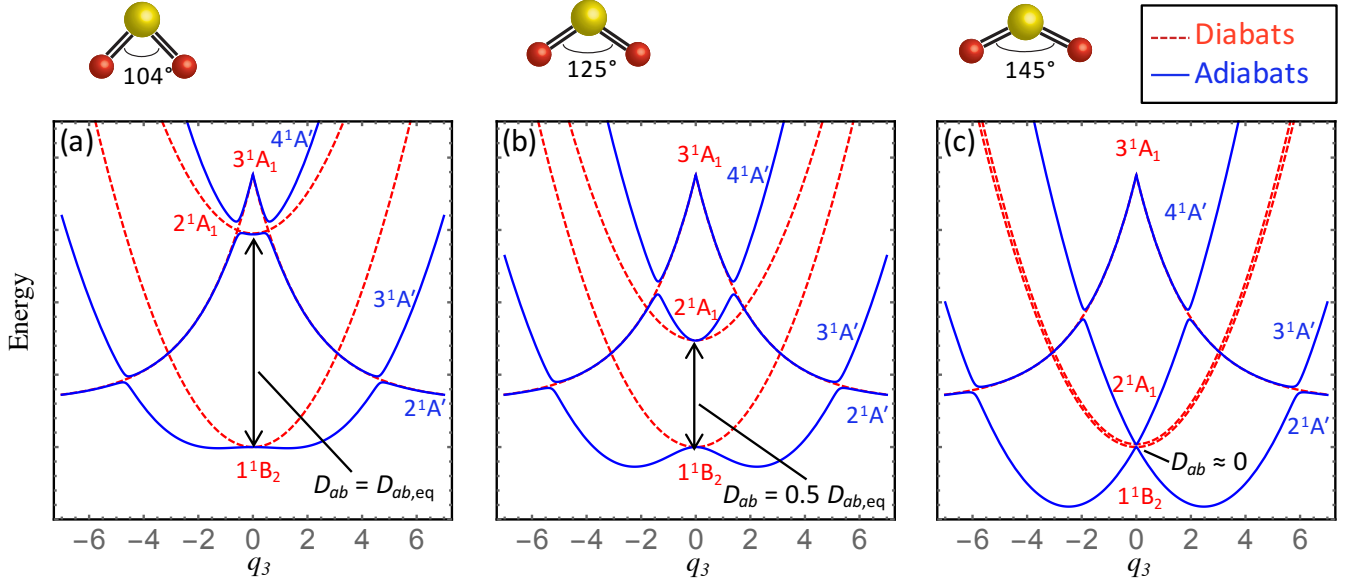


FIG. 4. A toy one-dimensional model for the  $q_3$ -mediated vibronic interaction between the  $1^1B_2$  ( $\tilde{C}$ ) state and the  $2^1A_1$  state is illustrated. The model is calculated from the Hamiltonian in Eq. (4) and is shown schematically as a function of  $D_{ab}$ , which gives the separation between the two bound diabatic states. Interaction with the dissociative  $4^1A'$  state is also included. The values of the parameters, in  $\text{cm}^{-1}$ , are  $D_{ab,\text{eq}} = 14760$ ,  $D_{ac} = 18792$ ,  $D_0 = 3152$ ,  $\lambda_{ab} = 3400$ ,  $\lambda_{bc} = 500$ ,  $\omega_3 = 1350$ , and the unitless parameter  $l = 2$ . The two bound potential energy surfaces cross via a conical intersection that occurs at a bond angle of  $\sim 145^\circ$ , but the crossing is avoided at  $C_s$  geometries. Therefore, as the bond angle increases, the energy denominator for the vibronic interaction decreases and the effective barrier in the  $\tilde{C}$ -state adiabatic potential energy surface increases, consistent with the observations shown in Figure 2.

predicts a nearly linear increase in  $\Delta\omega_s$  of  $5.3 \text{ cm}^{-1}$  per quantum of  $v_2$ , whereas the experimentally determined trend is  $4.4 \text{ cm}^{-1}$  per quantum. The experimental trend in  $\Delta\omega_s(0, v_2)$  is thus consistent with the proposed vibronic interaction model, and further illustrates the capability of low-lying features on the potential energy surface to provide information about phenomena that occur at much higher energy. In this case, the trend in vibrational level staggering induced by a spectator mode ( $v_2$ ) acts as an early warning signal that alerts us to the approach to a conical intersection as the geometry is displaced along that mode.

We note that this type of effect, involving a totally symmetric spectator mode, is unique to *pseudo* Jahn-Teller systems, where a vibronic interaction between *non-degenerate* electronic states leads to a distorted minimum-energy configuration. In this type of system, the two electronic states are—in general—not degenerate, even at the symmetric configuration involving zero displacement along the non-totally symmetric coordinate, but may cross at a seam of conical intersection that occurs for particular displacements along the totally symmetric coordinates. In a *true* Jahn-Teller system, involving degenerate zero-order electronic states, totally symmetric spectator mode effects are not expected to occur, because the electronic states are necessarily degenerate at *any* configuration of the higher-symmetry point group of the zero-order states (i.e. at configura-

TABLE II. The vibrationally-averaged electronic state separation,  $\langle D_{ab}(v_2) \rangle$ , from Eq. (5–6), and the resulting value of the staggering parameter,  $\Delta\omega_s(0, v_2)$ , obtained from the vibronic coupling model (Eq. (2)), with  $D_{ab} = \langle D_{ab}(v_2) \rangle$  (Eq. (6)). The increase in  $\Delta\omega_s(0, v_2)$  per quantum of  $v_2$ ,  $\Delta\Delta\omega_s(0, v_2) = \Delta\omega_s(0, v_2) - \Delta\omega_s(0, v_2 - 1)$ , is also tabulated. The experimentally-determined  $\Delta\omega_s(0, v_2)$  and  $\Delta\Delta\omega_s(0, v_2)$  values are listed for comparison. All energies are in  $\text{cm}^{-1}$  units.

$v_2$	Model			Expt.	
	$\langle D_{ab}(v_2) \rangle$	$\Delta\omega_s(0, v_2)$	$\Delta\Delta\omega_s(0, v_2)$	$\Delta\omega_s(0, v_2)$	$\Delta\Delta\omega_s(0, v_2)$
0	14760	44.66		68.02	
1	14630	49.51	4.85	72.52	4.50
2	14497	54.85	5.34	76.65	4.13
3	14362	60.68	5.83	81.23	4.58

tions involving arbitrary displacement along the totally symmetric coordinates, but zero displacement along the non-totally symmetric coordinate.)

Our results support our proposed vibronic coupling mechanism with the  $2^1A_1$  state and also provide predictions against which to test theoretical investigations. To our knowledge, calculation of a full dimensional PES for the interacting  $1^1B_2$  ( $\tilde{C}$ ) and  $2^1A_1$  states has not been performed, and the location of the conical intersection as a function of  $q_1$  has not been investigated. However, if the decrease in  $\Delta\omega_s(v_1, 0)$  (see Fig. 2) is influenced by



the location of the seam of conical intersection in a similar manner as the trend in  $\Delta\omega_s(0, v_2)$ , this would suggest that at the  $\tilde{C}$  state equilibrium bond angle, the conical intersection occurs at *shorter* than the effective  $C_{2v}$  equilibrium bond distance of 1.576 Å. That is, as the effective bond lengths are increased, the strength of the vibronic interaction decreases, indicating an increase in the energy denominator for the vibronic interaction.

#### IV. CONCLUSIONS

Our observations (reported in Part I of this series)<sup>21</sup> are consistent with a vibronic coupling model for the asymmetric equilibrium bonding structure, first proposed by Innes,<sup>24</sup> in which the  $\tilde{C}$  state undergoes a  $q_3$ -mediated interaction with the (diabatically) bound  $2^1A_1$  state. The oscillator strength of the  $2^1A_1 \leftarrow \tilde{X}^1A_1$  transition is calculated to be relatively weak at the equilibrium  $C_{2v}$  geometry, which is consistent with the fact that no vibronically-allowed one-photon transitions to low-lying  $b_2$  vibrational levels of the  $\tilde{C}$  state have been observed. As noted in Ref. 9, vibronically allowed transitions that violate the vibrational selection rules are plausible at higher energies near the avoided crossing of the  $\tilde{C}$ -state with  $2^1A_1$  in the dissociative region, because  $2^1A_1$  probably borrows oscillator strength via an avoided crossing with the dissociative  $3^1A_1$  state.

Using information from the low-lying vibrational levels of the  $\tilde{C}$ -state, we are able to develop a picture that accounts for these three interacting electronic states. Our one-dimensional two-state vibronic model fails to reproduce the observed level pattern in the  $(0, 0, v_3)$  progression unless an anomalously low value of  $\omega'_3$  is chosen for the upper state. This may suggest an indirect role that the repulsive  $3^1A_1$  state plays in shaping the adiabatic  $\tilde{C}$ -state potential energy surface. Interaction of  $2^1A_1$  with  $3^1A_1$  may dramatically decrease the effective  $\omega'_3$  frequency of  $2^1A_1$ , giving rise to the low value of  $\omega'_3$  in our fit model. The apparent involvement of  $3^1A_1$  in the observed level structure has profound implications for the photodissociation dynamics of  $SO_2$ , since interaction of  $2^1A_1$  with the dissociative state gives rise to an avoided crossing with the  $\tilde{C}$  state, causing it to correlate adiabatically to the ground state  $SO(^3\Sigma^-) + O(^3P)$  product channel.<sup>4,5,8,9,12,13,25,26</sup>

We have also developed a model to explain quantitatively the increasing effective barrier height as a function of bending quantum number,  $v_2$ . As quanta of  $v_2$  are added, the effective bond angle increases and the geometry approaches that of the conical intersection with the  $2^1A_1$  state, calculated to occur at  $\sim 145^\circ$ . The model quantitatively reproduces the observed increase in level staggering of the  $v_3$  progression as a function of  $v_2$  ( $\sim 5\text{ cm}^{-1}$  per quantum of  $v_2$ ). Our work provides information against which to compare future *ab initio* calculations of the vibronic coupling around the equilibrium geometry of the  $\tilde{C}$  state.

Finally, our work demonstrates the ability of high-resolution spectroscopy on comparatively simple, low-lying vibrational energy levels to provide useful qualitative information about interactions that occur at much higher energies. The relative simplicity of these low-lying vibrational levels provides an advantage over spectroscopic experiments at higher energy, where assignments are often ambiguous if not impossible. We have used the low-lying vibrational structure in the  $\tilde{C}$  state of  $SO_2$  to identify signatures of a three-state vibronic interaction mechanism, as well as the approach toward a conical intersection along the bending coordinate.

#### V. ACKNOWLEDGMENTS

The authors thank Anthony Merer and John Stanton for valuable discussions. This material is based upon work supported by the U.S. Department of Energy, Office of Science, Chemical Sciences Geosciences and Biosciences Division of the Basic Energy Sciences Office, under Award Number DE-FG0287ER13671.

- <sup>1</sup>Masahiro Kawasaki, Kazuo Kasatani, Hiroyasu Sato, Hisanori Shinohara, and Nobuyuki Nishi. Photodissociation of molecular beams of  $SO_2$  at 193 nm. *Chemical Physics*, 73(3):377–382, 1982.
- <sup>2</sup>Hideto Kanamori, James E. Butler, Kentarou Kawaguchi, Chikashi Yamada, and Eizi Hirota. Spin polarization in SO photochemically generated from  $SO_2$ . *The Journal of Chemical Physics*, 83(2):611–615, 1985.
- <sup>3</sup>C.S. Effenhauser, P. Felder, and J. Robert Huber. Two-photon dissociation of sulfur dioxide at 248 and 308 nm. *Chemical Physics*, 142(2):311–320, 1990.
- <sup>4</sup>Kenshu Kamiya and Hiroyuki Matsui. Theoretical studies on the potential energy surfaces of  $SO_2$ : Electronic states for photodissociation from the  $\tilde{C}^1B_2$  state. *Bulletin of the Chemical Society of Japan*, 64(9):2792–2801, 1991.
- <sup>5</sup>S. Becker, C. Braatz, J. Lindner, and E. Tiemann. State specific photodissociation of  $SO_2$  and state selective detection of the SO fragment. *Chemical Physics Letters*, 208(1-2):15–20, 1993.
- <sup>6</sup>S. Becker, C. Braatz, J. Lindner, and E. Tiemann. Investigation of the predissociation of  $SO_2$ : state selective detection of the SO and O fragments. *Chemical Physics*, 196(1-2):275–291, 1995.
- <sup>7</sup>Akihiro Okazaki, Takayuki Ebata, and Naohiko Mikami. Degenerate four-wave mixing and photofragment yield spectroscopic study of jet-cooled  $SO_2$  in the  $\tilde{C}^1B_2$  state: Internal conversion followed by dissociation in the  $\tilde{X}$  state. *The Journal of Chemical Physics*, 107(21):8752–8758, 1997.
- <sup>8</sup>Hideki Katagiri, Tokuei Sako, Akiyoshi Hishikawa, Takeki Yazaki, Ken Onda, Kaoru Yamanouchi, and Kouichi Yoshino. Experimental and theoretical exploration of photodissociation of  $SO_2$  via the  $\tilde{C}^1B_2$  state: identification of the dissociation pathway. *Journal of Molecular Structure*, 413–414(0):589–614, 1997.
- <sup>9</sup>Paresh C. Ray, Michael F. Arendt, and Laurie J. Butler. Resonance emission spectroscopy of predissociating  $SO_2 \tilde{C} (1^1B_2)$ : Coupling with a repulsive  $^1A_1$  state near 200 nm. *The Journal of Chemical Physics*, 109(13):5221–5230, 1998.
- <sup>10</sup>Tokuei Sako, Akiyoshi Hishikawa, and Kaoru Yamanouchi. Vibrational propensity in the predissociation rate of  $SO_2(\tilde{C}^1B_2)$  by two types of nodal patterns in vibrational wavefunctions. *Chemical Physics Letters*, 294(6):571–578, 1998.
- <sup>11</sup>Daiqian Xie, Guobin Ma, and Hua Guo. Quantum calculations of highly excited vibrational spectrum of sulfur dioxide. III. Emission spectra from the  $\tilde{C}^1B_2$  state. *The Journal of Chemical Physics*, 111(17):7782–7788, 1999.

- <sup>12</sup>Brad Parsons, Laurie J. Butler, Daiqian Xie, and Hua Guo. A combined experimental and theoretical study of resonance emission spectra of  $\text{SO}_2(\tilde{\text{C}}^1\text{B}_2)$ . *Chemical Physics Letters*, 320(5–6):499–506, 2000.
- <sup>13</sup>Bogdan R. Cosofret, Scott M. Dylewski, and Paul L. Houston. Changes in the vibrational population of  $\text{SO}({}^3\Sigma^-)$  from the photodissociation of  $\text{SO}_2$  between 202 and 207 nm. *The Journal of Physical Chemistry A*, 104(45):10240–10246, 2000.
- <sup>14</sup>James Farquhar, Joel Savarino, Sabine Airieau, and Mark H. Thiemens. Observation of wavelength-sensitive mass-independent sulfur isotope effects during  $\text{SO}_2$  photolysis: Implications for the early atmosphere. *J. Geophys. Res.*, 106(E12):32829–32839, 2001.
- <sup>15</sup>Yuchuan Gong, Vladimir I. Makarov, and Brad R. Weiner. Time-resolved Fourier transform infrared study of the 193 nm photolysis of  $\text{SO}_2$ . *Chemical Physics Letters*, 378(5–6):493–502, 2003.
- <sup>16</sup>Jules Duchesne and B. Rosen. Contribution to the study of electronic spectra of bent triatomic molecules. *The Journal of Chemical Physics*, 15(9):631–644, 1947.
- <sup>17</sup>V. T. Jones and J. B. Coon. The ultraviolet spectrum of  $\text{SO}_2$  in matrix isolation and the vibrational structure of the 2348 Å system. *Journal of Molecular Spectroscopy*, 47(1):45–54, 1973.
- <sup>18</sup>J. C. D. Brand, P. H. Chiu, A. R. Hoy, and H. D. Bist. Sulfur dioxide: Rotational constants and asymmetric structure of the  $\tilde{\text{C}}^1\text{B}_2$  state. *Journal of Molecular Spectroscopy*, 60(1–3):43–56, 1976.
- <sup>19</sup>A. R. Hoy and J. C. D. Brand. Asymmetric structure and force field of the  ${}^1\text{B}_2({}^1\text{A}')$  state of sulphur dioxide. *Molecular Physics*, 36(5):1409–1420, 1978.
- <sup>20</sup>Karl-Eliv Johann Hallin. *Some aspects of the electronic spectra of small triatomic molecules*. PhD thesis, The University of British Columbia, 1977.
- <sup>21</sup>G. Barratt Park, Jun Jiang, Catherine A. Saladrigas, and Robert W. Field. Observation of  $b_2$  symmetry vibrational levels of the  $\text{SO}_2 \tilde{\text{C}}^1\text{B}_2$  state: Vibrational level staggering, Coriolis interactions, and rotation-vibration constants. *The Journal of Chemical Physics*, 144(14):144311, 2016.
- <sup>22</sup>Jun Jiang, G. Barratt Park, and Robert W. Field. The rotation-vibration structure of the  $\text{SO}_2 \tilde{\text{C}}^1\text{B}_2$  state explained by a new internal coordinate force field. *The Journal of Chemical Physics*, 144(14):144312, 2016.
- <sup>23</sup>R. S. Mulliken. The lower excited states of some simple molecules. *Canadian Journal of Chemistry*, 36(1):10–23, 1958.
- <sup>24</sup>K.K Innes.  $\text{SO}_2$ : Origins of unequal bond lengths in the  $\tilde{\text{C}}^1\text{B}_2$  electronic state. *Journal of Molecular Spectroscopy*, 120(1):1–4, 1986.
- <sup>25</sup>Petr Nachtigall, Jan Hrušák, Ota Bludský, and Suehiro Iwata. Investigation of the potential energy surfaces for the ground  $\tilde{\text{X}}^1\text{A}_1$  and excited  $\tilde{\text{C}}^1\text{B}_2$  electronic states of  $\text{SO}_2$ . *Chemical Physics Letters*, 303:441–446, 1999.
- <sup>26</sup>Ota Bludský, Petr Nachtigall, Jan Hrušák, and Per Jensen. The calculation of the vibrational states of  $\text{SO}_2$  in the  $\tilde{\text{C}}^1\text{B}_2$  electronic state up to the  $\text{SO}({}^3\Sigma^-)+\text{O}^3(\text{P})$  dissociation limit. *Chemical Physics Letters*, 318(6):607–613, 2000.
- <sup>27</sup>H. Okabe. Fluorescence and predissociation of sulfur dioxide. *Journal of the American Chemical Society*, 93(25):7095–7096, 1971.
- <sup>28</sup>Man-Him Hui and Stuart A. Rice. Decay of fluorescence from single vibronic states of  $\text{SO}_2$ . *Chemical Physics Letters*, 17(4):474–478, 1972.
- <sup>29</sup>J. C. D. Brand, D. R. Humphrey, A. E. Douglas, and I. Zanon. The resonance fluorescence spectrum of sulfur dioxide. *Canadian Journal of Physics*, 51:530, 1973.
- <sup>30</sup>Hong Ran, Daiqian Xie, and Hua Guo. Theoretical studies of absorption spectra of  $\text{SO}_2$  isotopomers. *Chemical Physics Letters*, 439(4–6):280–283, 2007.
- <sup>31</sup>Yong-feng Zhang, Mei-shan Wang, Mei-zhong Ma, and Rong-cai Ma. Ground and low-lying excited states of  $\text{SO}_2$  studied by the SAC/SAC-CI method. *Journal of Molecular Structure: THEOCHEM*, 859:7–10, 2008.
- <sup>32</sup>Ikuo Tokue and Shinkoh Nanbu. Theoretical studies of absorption cross sections for the  $\tilde{\text{C}}^1\text{B}_2-\tilde{\text{X}}^1\text{A}_1$  system of sulfur dioxide and isotope effects. *The Journal of Chemical Physics*, 132(2):024301, 2010.
- <sup>33</sup>Daiqian Xie, Hua Guo, Ota Bludský, and Petr Nachtigall. Absorption and resonance emission spectra of  $\text{SO}_2 \tilde{\text{X}}^1\text{A}_1/\tilde{\text{C}}^1\text{B}_2$  calculated from ab initio potential energy and transition dipole moment surfaces. *Chemical Physics Letters*, 329(5–6):503–510, 2000.
- <sup>34</sup>Michael H. Palmer, David A. Shaw, and Martyn F. Guest. The electronically excited and ionic states of sulphur dioxide: an *ab initio* molecular orbital CI study and comparison with spectral data. *Molecular Physics*, 103(6–8):1183–1200, 2005.